ACSNANO

www.acsnano.org

ARTICLE

# Uncovering the Mechanisms of Triplet–Triplet Annihilation Upconversion Enhancement via Plasmonic Nanocavity Tuning

Rachel E. Bangle, Hengming Li, and Maiken H. Mikkelsen*

Cite This: https://doi.org/10.1021/acsnano.3c08915

Read Online

ACCESS | Metrics & More | Article Recommendations | Supporting Information

**ABSTRACT:** The nonlinear conversion of photons from lower to higher energy is important for a wide range of applications, from quantum communications and optoelectronics to solar energy conversion and medicine. Triplet–triplet annihilation upconversion (TTA UC), which utilizes an absorber/emitter molecular pair, is a promising tool for upconversion applications requiring low intensity light such as photovoltaics, photocatalysis, and bioimaging. Despite demonstrations of efficient TTA UC in solution, practical applications have proven difficult, as thin films retard the necessary energy transfer steps and result in low emission yields. In this work, TTA UC emission from a thin film is greatly enhanced through integration into plasmonic nanogap cavities consisting of a silver mirror, a nanometer-scale polymer spacer containing a TTA molecular pair, and colloidally synthesized silver nanocubes. Mechanistic studies performed by varying the nanocube side length (45–150 nm) to tune the nanogap cavity resonance paired with simulations reveal absorption rate enhancement to be the primary operative mechanism in overall TTA UC emission enhancement. This absorption enhancement decreases the TTA UC threshold intensity by an order of magnitude and allows TTA UC emission to be excited with light up to 120 nm redder than the usable wavelength range for the control samples. Further, combined nanogap cavities composed of two distinct nanocube sizes result in surfaces which simultaneously enhance the absorption rate and emission rate. These dual-size nanogap cavities result in 45-fold TTA UC emission enhancement. In total, these studies present TTA UC emission enhancement, illustrate how the usable portion of the spectrum can be expanded for a given sensitizer–emitter pair, and develop both mechanistic understanding and design rules for TTA UC emission enhancement by plasmonic nanostructures.

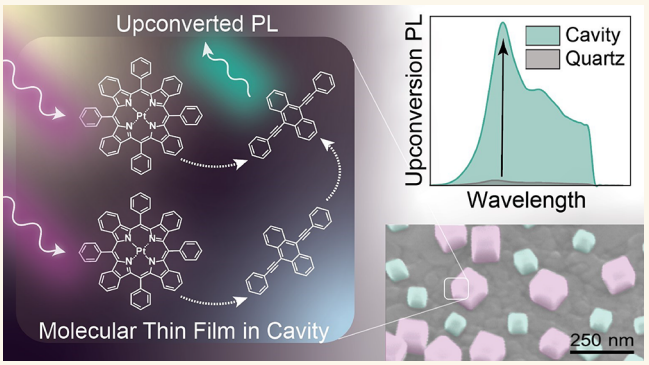


**KEYWORDS:** *triplet–triplet annihilation, upconversion, plasmonics, nanocavities, photoluminescence*



## INTRODUCTION

Upconversion (UC), i.e. conversion of multiple low-energy photons into a single higher-energy photon, affords flexibility to photochemical and photonic systems.[1−5] For example, UC can allow photovoltaic cells to overcome the Schockley–Queisser limit,[6] improve the performance of organic light emitting diodes,[7] or expand the spectral range of solar photocatalysis.[8] Upconversion materials can absorb tissue-penetrating IR light and emit visible wavelengths for biological imaging[9] or molecular light therapy.[10] Recent work has also used UC to initiate polymerization for 3D printing.[11] Despite this promise, UC emission brightness is frequently low because of compounding loss pathways within the multiple absorption and energy transfer steps.[12]

A common upconversion strategy is triplet–triplet annihilation (TTA), a multimolecular process in which an absorber molecule forms an excited triplet which undergoes energy transfer with an emitter molecule, which then undergoes TTA to form a high-energy, emissive singlet state (Figure 1).[1] Synthetic tunability allows spectral diversity, and absorption coefficients can be relatively large.[5] Solution TTA UC efficiencies have, however, proven difficult to translate into technologically useful UC films, as energy transfer steps generally require short intermolecular distances (<1 nm)

Received: September 17, 2023
Revised: November 13, 2023
Accepted: November 15, 2023

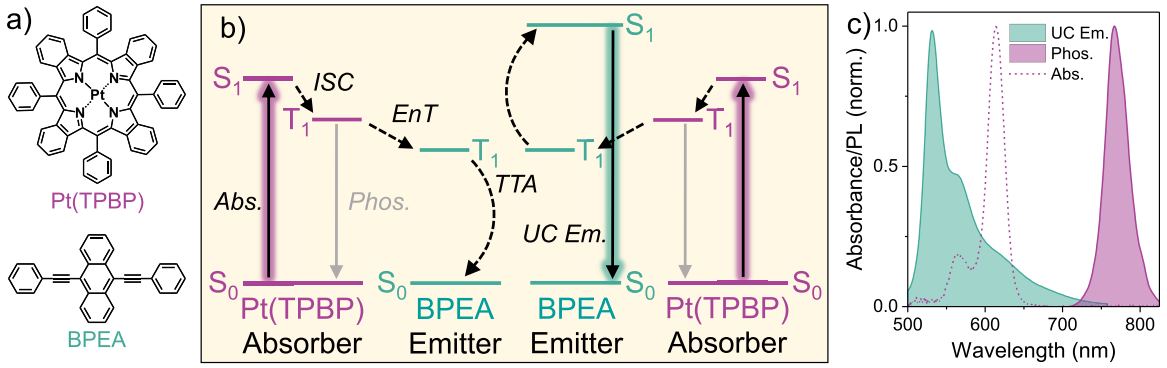


**Figure 1. (a) Absorber and emitter molecules known to undergo triplet−triplet annihilation (TTA) upconversion. (b) Schematic representation of upconversion within the utilized molecules. Red light absorption by Pt(TPBP) is followed by intersystem crossing (ISC). The resulting triplet can undergo energy transfer (EnT) with neighboring BPEA. Two adjacent BPEA triplets can undergo TTA to form a singlet that radiatively decays to produce green upconverted emission (UC Em.). (c) Pt(TPBP) absorption (dashed) and relevant emission (solid)—BPEA UC Em. and Pt(TPBP) phosphorescence (Phos).**

within diffusion-limited encounter complexes[12−15] or elaborate self-assembly to create energy transfer pathways.[16,17] As such, increased UC brightness is vital to implementing TTA UC films.

Plasmonic nanostructures can increase molecular emission brightness, as strong electric fields enhance both absorption and emission.[18,19] Though UC emission has been enhanced, studies have largely focused on upconversion within lanthanide-doped nanoparticles.[4,20] Nanoplasmonic enhancement of the TTA UC has been limited, and rate-limiting energy transfer steps raise questions as to the efficacy of absorption or emission enhancement. To date, TTA UC emission brightnesshas been increased less than an order of magnitude by plasmonic nanostructures.[21−23] Baldo and coworkers have achieved larger TTA UC emission enhancement (227-fold) in a distributed Bragg reflector microcavity by improving absorption, but in this work limited cavity resonance tunability (<100 nm) lessens the ability to explore alternative enhancement mechanisms.[24]

In this paper, we integrate a TTA system into colloidally fabricated plasmonic nanogap cavities. Through spectral tuning of the cavity resonance, we achieve UC emission brightness enhancement and expand the range of possible excitation wavelengths. Combinations of nanogap cavities create surfaces with two resonances which influence both absorption and emission and result in maximized brightness with 45-fold enhancement. Mechanistic investigation shows that bright UC largely results from increased absorption, which illustrates design rules for further TTA UC plasmonic enhancement. In this article, experimental results are presented first, followed by a discussion of mechanistic implications supported by simulations.

## RESULTS

**Nanogap Cavities.** Platinum(II) 5,10,15,20-(tetraphenyl)-tetrabenzoporphyrin (Pt(TPBP)), and 9,10-bis-(phenylethynyl)anthracene (BPEA) absorber and emitter molecules are integrated into plasmonic nanogap cavities.[25] Red photon absorption by Pt(TPBP) generates an excited triplet ($T_1$) through rapid intersystem crossing (Figure 1).[26] When in very close proximity, Pt(TPBP) $T_1$ and BPEA undergo spontaneous energy transfer to generate a BPEA $T_1$ state not accessible through direct excitation.[25,27] When two BPEA $T_1$ molecules encounter each other, they undergo triplet−triplet annihilation (TTA) to form a high-energy singlet ($S_1$), which decays through green photon emission. This represents an ∼85 nm (0.32 eV) apparent anti-Stokes shift, i.e. the difference between the Pt(TPBP) absorption and BPEA emission peaks (Figure 1c).

Nanogap cavities (Figure 2a-b) fabricated with bottom-up techniques require no costly lithography steps (see Methods).[18,19,28] Colloidally synthesized silver nanocubes are separated from a silver mirror by a spin-coated spacer layer, called a "gap," made of poly(vinyl alcohol) (PVA) and poly(methyl methacrylate) (PMMA). The TTA molecules (3 mM BPEA and 0.3 mM Pt(TPBP)) are dispersed in a 6 nm PMMA layer, and an interposed PVA film significantly reduces nonradiative quenching by the mirror. Emission brightness is maximized with 6 nm PVA (Figure S1). This is consistent with previous work which demonstrated that thicker gaps simultaneously increase emission quantum yields by preventing nonradiative quenching and decrease field enhancement such that emission brightness is maximized at an intermediate gap thickness.[19] An ∼1 nm layer of positively charged poly-(allylamine hydrochloride) (PAH) grown *in situ* on the PMMA electrostatically adheres to nanocubes coated in negatively charged polyvinylpyrrolidone (PVP) as described previously.[28,29] Cubes are deposited conformally over 20 $mm^2$ areas with an ∼13 nm total gap thickness to create a surface akin to a metasurface with ∼20% nanocube surface coverage. The surface is coated in thick (∼500 nm) PVA and stored in vacuum between experiments to exclude oxygen and prevent triplet quenching (Figure S2).

Reflection spectra of the cavity-coated surfaces exhibit a stark (85−90%) decrease in reflectivity at the resonant wavelength (Figure 2e) as measured through a 20× objective with a 1.1 mm diameter field of view (Methods). The samples are optically thick, and previous work has shown that nanogap cavity-coated surfaces such as these scatter <1% of incident resonant light.[29] As such, dips in the reflectance spectra indicate that the cavities are strong light absorbers. These nanogap cavities interact with light by way of gap-plasmon modes, in which the film plasmon and nanocube plasmon hybridize to a single cavity mode which reflects repeatedly at the nanocube edges in a Fabry−Perót-like resonance. The structure behaves as a grounded patch antenna, as has been theoretically described previously.[30−32] This confines resonant light tightly within the small volume of polymer underneath


https://doi.org/10.1021/acsnano.3c08915
ACS Nano XXXX, XXX, XXX−XXX

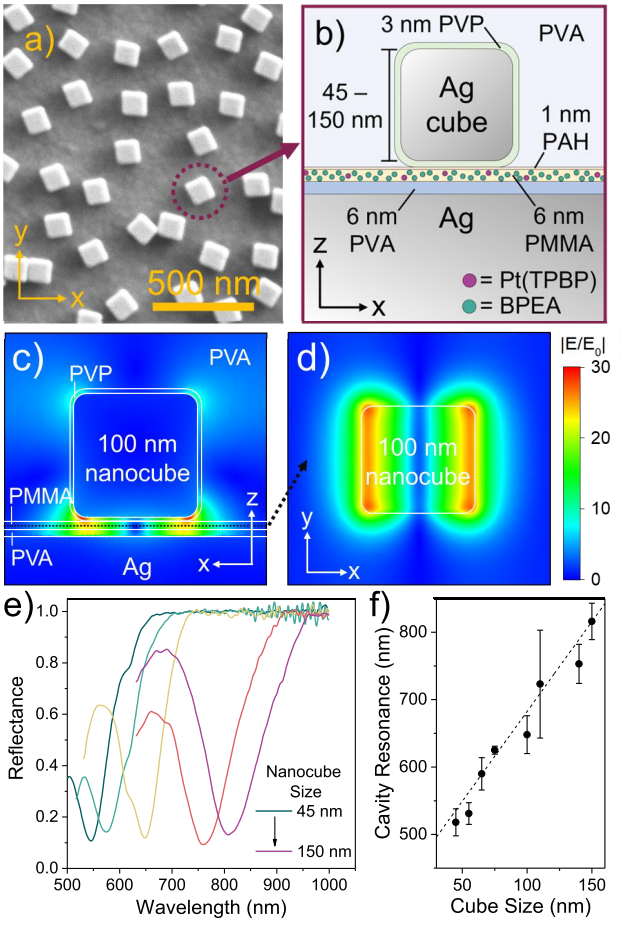


**Figure 2. (a) SEM image of Ag nanocubes on a flat Ag mirror (top view). (b) Schematic representation of a single nanogap cavity (side view). A 75 nm Ag mirror is spin coated with 6 nm of PVA and then 6 nm of PMMA into which BPEA and Pt(TPBP) are dissolved. A 1 nm PAH layer electrostatically adheres to the nanocubes ranging from 45−150 nm. A thick PVA topcoat excludes oxygen. (c-d) Finite-element simulations of the electric field enhancement $|E/E_0|$ within a single nanogap cavity upon resonant 630 nm excitation (TE polarized). An $x-z$ cross section is shown in (c). An $x-y$ plane representing the typical environment of the molecules at the position of the black dotted line is shown in (d). (e) Reflectance spectra of nanogap cavity-coated surfaces, including integrated BPEA and Pt(TPBP) molecules, over a circular area with 1.1 mm diameter. Nanocube side lengths are (left to right) 45, 55, 75, 110, and 150 nm. (f) The shift in cavity resonance as a function of nanocube side length from 45−150 nm.**

the cube, termed the gap.[19,29,30,33] As such, molecules in the gap experience extreme electric fields upon resonant cavity excitation, especially at the nanocube edges, as shown through finite-element simulations (Figure 2c-d). The cavity resonance is determined by the thickness and refractive index of the gap material and by the nanocube side length.[29,30] Synthetic tunability of the nanocubes,[28,34,35] here 45−150 nm side lengths, allows the resonance of the cavity-coated surfaces ($\lambda_c$) to be tuned nearly continuously from 500−815 nm with a single gap thickness (Figure 2e-f). Nanocubes of a given nominal size exhibit a side length coefficient of deviation <15% (purchased from nanoComposix). The addition of molecules results in only small shifts in $\lambda_c$ (Figure S3). Nanocube surface coverage densities of 19.2 ± 2.1% (Table S1) are determined by scanning electron microscopy (SEM). Because electrostatic repulsion between the charged PVP coating the nanocubes discourages close packing, ~ 20% nanocube loading represents surface density saturation previously shown to result in maximized surface absorption.[29] This places the largest possible portion of the TTA molecules in a nanogap cavity.

**Upconverted Emission.** Upconverted emission from the thin films upon continuous-wave 633 nm excitation is measured through a microscope objective in a reflective configuration (Figure S4, details in Methods). Emission is collected from the entire excited area (~210 $\mu$m diameter at fwhm) which comprises randomly distributed cavities with ~20% surface coverage and the thin film surface between cavities. The observed emission is shown to result from upconversion, as 633 nm excitation of BPEA without Pt(TPBP) results in negligible photoluminescence (PL) (Figure S5). Upconverted emission was considerably brighter from nanogap cavity-coated surfaces than from control samples consisting of equivalent polymer layers (6 nm PVA + 6 nm PMMA containing TTA molecules + ~500 nm PVA overlayer) on either a quartz substrate or a silver mirror with no nanocubes (Figure 3a). Quartz samples were mounted to a silver mirror to enable reflectance measurements and to account for increased Pt(TPBP) absorption due to the reflection of incident light. The structures of nanogap cavity and control samples are shown in Figure 3g.

Increased emission brightness from cavity-coated surfaces is quantified through the enhancement factor (EF), the ratio of integrated PL area from the cavity or silver samples vs the quartz control sample. Spectra are integrated over wavelengths 500−580 nm to avoid laser scatter sometimes observed in cavity-coated surfaces (for example Figure S5).

$$\mathrm{EF} = \frac{PL\ Area_{sample}}{PL\ Area_{quartz}} \quad (1)$$

At best, cavity-coated surfaces result in an EF of 35, while TTA UC emission from a silver substrate without nanocubes exhibits an EF of 6.3 ± 3.8. It should be noted that this EF is reported for 200 $\mu$W (580 mW/cm$^2$) excitation power at 633 nm. Values of EF vary with both excitation power and wavelength, as will be discussed further below. As such, comparisons within the literature should be made judiciously. This excitation power is in the linear power dependence regime for both cavity and quartz samples (Figure 3b). The TTA intensity threshold ($I_{th}$), i.e. the excitation power at which the rate limiting step changes from triplet−triplet annihilation to sensitizer-to-emitter energy transfer, is indicated by a transition from quadratic to linear power dependence.[13] When visualized on a log−log plot, this appears as a change in slope from 2 to 1. For cavity-coated surfaces, $I_{th}$ = 2.7 ± 0.6 mW/cm$^2$ is observed, which is nearly an order of magnitude smaller than that observed on a quartz sample, where $I_{th}$ = 24.5 ± 0.5 mW/cm$^2$, comparable to literature for similar sensitizer/emitter pairs in a solid matrix.[36]

Though TTA UC emission is enhanced for cavity-coated surfaces of all nanocube side lengths, the brightness depends heavily on the cavity resonance, $\lambda_c$ (Figure 3c-d). Maximized enhancement occurs when $\lambda_c$ is resonant with Pt(TPBP) absorption ($\lambda_{abs}$ = 615 nm), while both higher and lower $\lambda_c$ result in decreased EF. Notably, cavity-coated samples in resonance with BPEA emission ($\lambda_{em}$ = 530 nm) produce EF ≈ 15—less than half the maximum observed enhancement in


https://doi.org/10.1021/acsnano.3c08915
ACS Nano XXXX, XXX, XXX−XXX

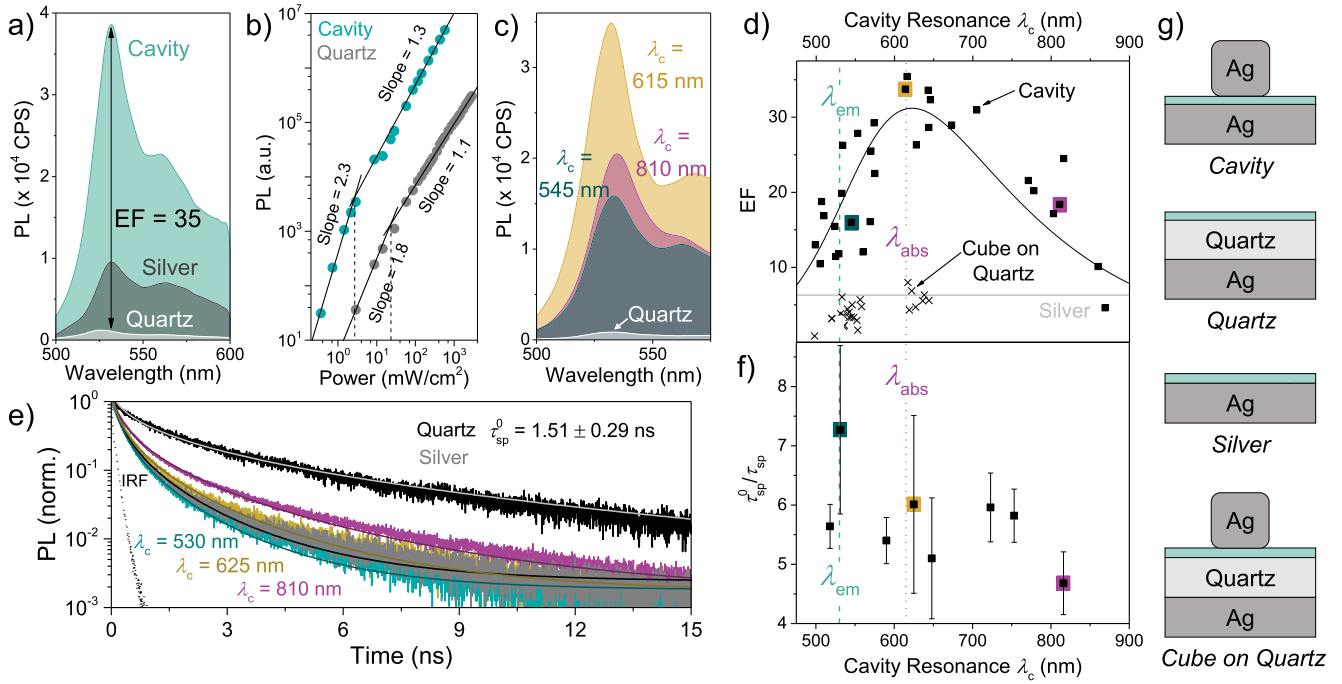


**Figure 3. (a) PL spectra upon 633 nm excitation showing TTA UC emission with EF = 35 for a cavity-coated surface with $\lambda_c$ = 619 nm. (b) Integrated PL intensity upon 633 nm excitation for a cavity-coated surface with $\lambda_c$ = 619 nm and a quartz control as a function of incident power. Linear fits determine the intensity thresholds (dashed lines). (c) PL spectra upon 633 nm excitation for cavity-coated surfaces with the indicated $\lambda_c$. (d) TTA UC emission EF (solid squares) as a function of $\lambda_c$. The largest EF is observed when $\lambda_c$ aligns with $\lambda_{abs}$ rather than $\lambda_{em}$. The data are fit with an asymmetrical peak (solid line) to guide the eye. Data points with color overlays correspond to the PL spectra in (c). Upconverted emission from control samples is also shown for silver (gray line) and nanocubes on quartz (crosses). (e) BPEA emission kinetics upon pulsed 440 nm excitation for BPEA films (no Pt(TPBP)) on quartz, silver, and cavity-coated surfaces with the indicated $\lambda_c$. Spontaneous emission lifetimes $\tau_{sp}$ are determined from stretched exponential fits ($\beta$ = 0.42) as described in SI. (f) Enhancement of $\tau_{sp}$ decreases as a function of $\lambda_c$. Data points with color overlays correspond to kinetic data in (e). Error bars are standard deviations between samples. (g) Sample structures (sizes not drawn to scale). Teal areas represent polymer layers containing TTA molecules. All samples are coated with an ~500 nm PVA layer (not shown).**

cavity-coated samples resonant with $\lambda_{abs}$. Shifts in $\lambda_c$ produce only small (<5 nm or 0.02 eV) shifts in $\lambda_{em}$ (Figure S6).

Additionally, upconverted emission was measured from control samples in which nanocubes were deposited onto polymer films on quartz mounted on a silver mirror (Figure S7, Figure 3g). Reflectance spectra of these nanocube on quartz samples exhibit significant broadband scattering (~80%) and weak absorbance peaks (Figure S7a). Finite element simulations show these peaks to be associated with absorbance by the cube, where the generated fields are located at the cube's top edges. As such, electric field enhancement within the layer of TTA molecules is minimal (Figure S7c-d). The peak wavelength associated with the cubes exhibits weak dependence on side length, ranging from ~500 to 650 nm (Figure S7b). The integrated PL area of upconverted emission from these nanocubes on quartz samples relative to quartz controls is shown as cross marks in Figure 3d. Enhancement generally increases with resonance wavelength to a maximum of EF = 8.

The spontaneous emission lifetime of BPEA ($\tau_{sp}$) is quantified by time-correlated single photon counting (Figure 3e, experimental details in Methods and Figure S8). Here, BPEA is directly excited with 440 nm pulsed light to remove the kinetic complications of energy transfer and TTA steps, and no Pt(TPBP) is present. On quartz, silver, and cavity-coated surfaces, BPEA emission exhibits stretched exponential kinetics (eq 8 in Methods) well-described with a stretching parameter of $\beta$ = 0.42. A deviation from single-exponential decay such as this is common in nanocavity enhanced emission[19,37,38] and likely results from the heterogeneous environments captured within the 210 $\mu$m diameter excitation area. Stretched exponential fits allow quantification of average lifetimes, which are taken as approximations of the BPEA spontaneous emission lifetimes $\tau_{sp}$ (see Methods, eq 9). This reveals that the BPEA $\tau_{sp}$ decreases for cavity-coated surfaces relative to the quartz controls (Table S2), quantified as $\tau_{sp}^0/\tau_{sp}$. On quartz, BPEA exhibits $\tau_{sp}^0$ of 1.51 ± 0.29 ns. For cavity-coated surfaces, the fastest BPEA emission with $\tau_{sp}$ = 0.21 ± 0.04 ns ($\tau_{sp}^0/\tau_{sp} \approx 7$) occurs from samples coated with $\lambda_{em}$-resonant cavities, though $\tau_{sp}$ displays only a weak dependence on $\lambda_c$ (Figure 3f). In general, $\tau_{sp}$ decreases as $\lambda_c$ shifts to lower energies, but the change is similar in magnitude to the standard deviations between measurements (Figure 3f). Further, similar decreases in $\tau_{sp}$ are observed for cavity-coated surfaces and silver surfaces without nanocubes, for which $\tau_{sp}$ = 0.19 ± 0.01 ns (Figure 3e, Table S2).

Photoluminescence excitation (PLE) spectra quantify the TTA UC emission measured at a single wavelength (530 nm) upon pulsed (~200 fs) laser excitation from a tunable OPO as a function of excitation wavelength (details in Methods). Control samples on quartz exhibit PLE spectra which closely follow the Pt(TPBP) absorption spectrum (Figure 4a, Figure S9), while silver samples and cavity-coated surfaces with $\lambda_c$ = 600 nm exhibit slight PLE broadening. In contrast, cavity-coated surfaces with $\lambda_c$ = 670 nm produce broadened PLE spectra with measurable TTA UC emission intensity upon


https://doi.org/10.1021/acsnano.3c08915
ACS Nano XXXX, XXX, XXX−XXX

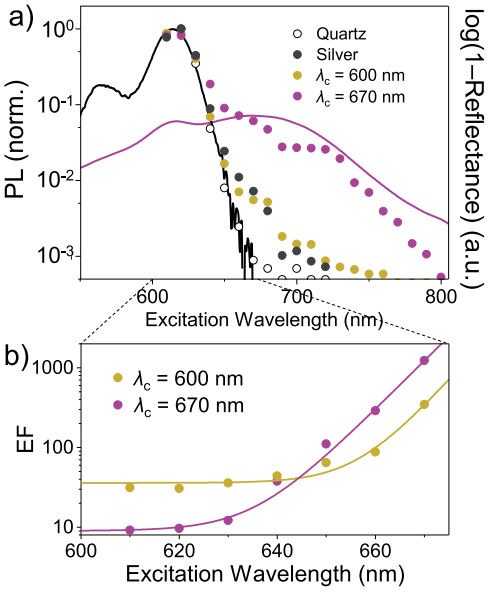


**Figure 4. (a) Normalized PL intensity (points, left axis) measured at 530 nm as a function of excitation wavelength from quartz, silver, and cavity-coated surfaces with the indicated $\lambda_c$. The Pt(TPBP) absorption (black, right axis) and nanogap cavity inverted reflectance (purple, right axis) are overlaid. Both axes are plotted logarithmically. (b) Enhancement factor (EF) of the cavities in (a) as a function of excitation wavelength.**

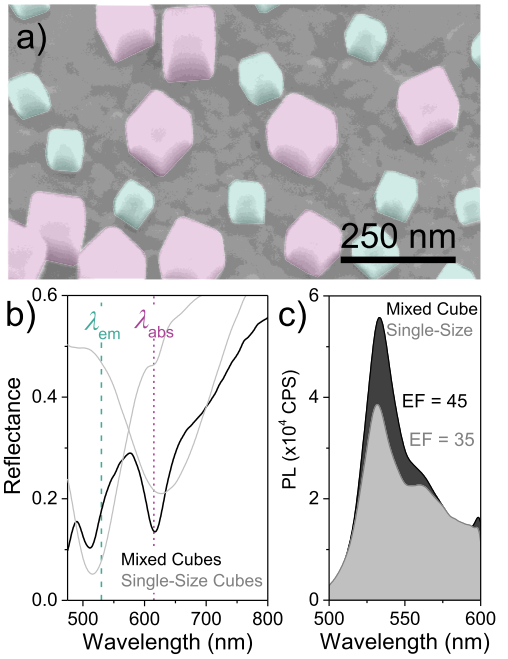


**Figure 5. (a) False-color SEM image of nanocavities tilted 40° consisting of two nominal nanocube sizes, 65 (turquoise) and 100 nm (pink). (b) Reflectance spectrum of a silver surface coated in a mixture of nanogap cavities with two side lengths results in dual resonances aligned with $\lambda_{em}$ and $\lambda_{abs}$ (black). The reflectance spectra of each individual nanocube size are overlaid (gray). (c) PL spectra of UC emission upon 633 nm excitation of BPEA + Pt(TPBP) integrated into a cavity-coated surface with single or mixed cube sizes.**

excitation that is up to 120 nm redder than the quartz control sample. Notably, this PLE broadening roughly corresponds with the absorbance spectra of the cavity-coated surface. Because the PLE of the control sample decreases with excitation wavelength more rapidly than does PLE from the cavity-coated surfaces, the effective enhancement factor increases as excitation shifts red (Figure 4b).

To explore the impact of nanogap cavity resonances which overlap with both $\lambda_{abs}$ and $\lambda_{em}$, a dual-resonance cavity-coated surface is fabricated. Colloidal deposition of a nanocube mixture consisting of equal weights 65 and 100 nm nanocubes results in well-dispersed nanogap cavities of both sizes with ~20% total surface coverage density (Figure 5a). Reflectance spectra of these surfaces exhibit two resonance peaks, consistent with a summation of the resonances of the single-size nanogap cavity-coated surfaces (Figure 5b). Integration of TTA UC molecules into these dual-resonance surfaces results in brighter emission upon 633 nm, 580 mW/cm$^2$ CW excitation than did any single size nanogap cavity surface, with EF ≈ 45 (Figure 5c).

**Pt(TPBP) Phosphorescence.** In addition to TTA UC emission, phosphorescence from Pt(TPBP) is brightened on cavity-coated surfaces. Phosphorescence brightness resulting from 580 mW/cm$^2$ 633 nm excitation (Figure 6a) depends heavily on $\lambda_c$, where EF is maximized (EF ≈ 65) for $\lambda_c$ = 770 nm. Phosphorescence lifetimes display a nearly identical $\lambda_c$ dependence, where $\tau_{sp}$ is most decreased when $\lambda_c$ = 750 nm with $\tau_{sp}$ = 56 ± 2 ns ($\tau_{sp}^0/\tau_{sp}$ = 207). This is determined from phosphorescence kinetics of Pt(TPBP) films containing no BPEA in cavity-coated surfaces which exhibit prominent fast and slow components. The fast component dominates at $t$ < 2 μs (Figure 6b), and PL decay on this time scale is fit with a stretched exponential function with $\beta$ = 0.39 to approximate $\tau_{sp}$ (Table S3). This lifetime is compared to the lifetime attained for Pt(TPBP) phosphorescence on quartz, which displays no fast component ($\tau_{sp}^0$ = 11.6 ± 1.6 μs) (Figure S10). Notably, and in contrast to TTA UC emission, maximum phosphorescence EF and minimum $\tau_{sp}$ occur when cavity-coated surfaces are approximately resonant with the phosphorescence wavelength ($\lambda_{phos}$ = 765 nm) (Figure 6c). Both higher and lower $\lambda_c$ result in significantly smaller brightness and longer $\tau_{sp}$, and cavity-coated surfaces in resonance with $\lambda_{abs}$ produce roughly half of the maximum effect (EF ≈ 30 and $\tau_{sp}^0/\tau_{sp}$ ≈ 95). Also in contrast to BPEA emission, Pt(TPBP) phosphorescence lifetimes are nearly identical for quartz and silver samples, where for silver, $\tau_{sp}$ = 14.3 ± 1.0 μs.

## DISCUSSION

Integration of a TTA UC emission molecular pair into nanogap cavity-coated surfaces resulted in 35-fold upconversion emission brightness enhancement, and the observed cavity resonance dependence provides information with regards to the operative mechanism(s). Nanogap cavity-coated surfaces such as these have previously been shown to result in extreme photonic environments within the gap which alter molecular emission brightness and lifetimes through several intertwined mechanisms.[18,29,39,40] Traditionally, emission brightness enhancement within nanocavities as a function of cavity resonance $\lambda_c$ is summarized in an emission enhancement factor,

$$EF_{em}(\lambda_c) = \frac{\eta(\lambda_c)\kappa_{abs}(\lambda_c)\Phi_{em}(\lambda_c)}{\eta^0\kappa_{abs}^0\Phi_{em}^0} \quad (2)$$


https://doi.org/10.1021/acsnano.3c08915
ACS Nano XXXX, XXX, XXX−XXX

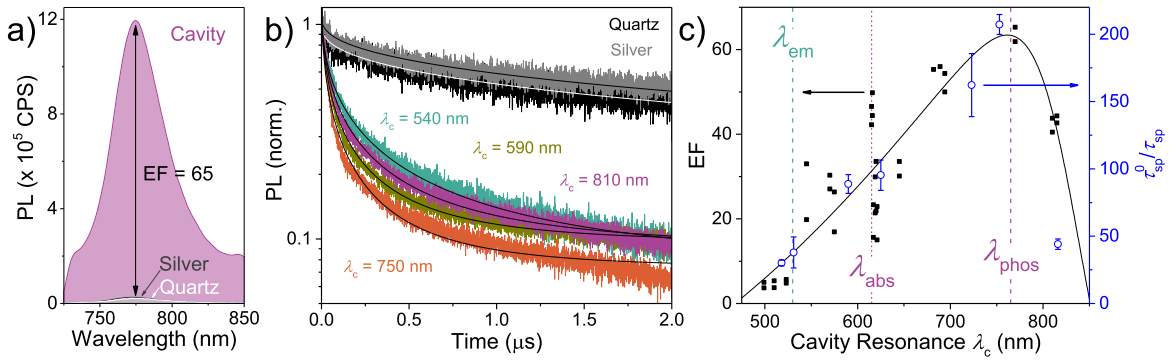


**Figure 6. (a) PL spectra upon 633 nm CW excitation of a cavity sample with $\lambda_c$ = 770 nm and quartz and silver controls exhibiting Pt(TPBP) phosphorescence with EF = 65. (b) Pt(TPBP) phosphorescence kinetics upon pulsed 633 nm excitation for Pt(TPBP) films (no BPEA) on quartz, silver, and cavity-coated surfaces with the indicated $\lambda_c$. Spontaneous emission lifetimes $\tau_{sp}$ are determined from stretched exponential fits ($\beta$ = 0.39). (c) Measured phosphorescence EF (black squares) and $\tau_{sp}^0/\tau_{sp}$ (open blue circles) as a function of $\lambda_c$. The data are fit with an asymmetrical double sigmoidal peak (solid line) to guide the eye.**

$$\Phi_{em}(\lambda_c) = \frac{1/\tau_r(\lambda_c)}{1/\tau_r(\lambda_c) + 1/\tau_{nr}(\lambda_c)} = \frac{1/\tau_r(\lambda_c)}{1/\tau_{sp}(\lambda_c)} \quad (3)$$

Here $\eta$ is the objective collection efficiency; $\kappa_{abs}$ is the absorption rate, i.e. the number of molecules excited per unit time; $\Phi_{em}$ is the emission quantum yield defined by the radiative and nonradiative excited state decay lifetimes $\tau_r$ and $\tau_{nr}$; and the superscript "0" indicates the values of a quartz control sample.[19,33,41] It should be noted that each parameter displays a distinct dependence on $\lambda_c$. Additionally, large scattering cross sections in nanoparticles can increase the number of interactions between molecular absorbers and photons,[42] and light-induced heating of plasmonic nanoparticles can increase the vibrational decay of proximate molecular excited states.[43] While this picture has accurately modeled experimental results for simple fluorophores,[18] additional processes must also be considered within a TTA system. The upconversion emission quantum yield $\Phi_{UCem}$ depends on the quantum yields of the intersystem crossing ($\Phi_{ISC}$), energy transfer ($\Phi_{EnT}$), and triplet−triplet annihilation ($\Phi_{TTA} \leq 1/2$) and the likelihood of forming a singlet state as opposed to triplet or quintet states upon TTA ($f$) in addition to $\Phi_{em}$ from the emitter.[12,44,45]

$$\Phi_{UCem} = f\Phi_{em}\Phi_{ISC}\Phi_{EnT}\Phi_{TTA} \quad (4)$$

$$EF_{UCem}(\lambda_c) = \frac{\eta(\lambda_c)\kappa_{abs}(\lambda_c)\Phi_{UCem}(\lambda_c)}{\eta^0\kappa_{abs}^0\Phi_{UCem}^0} \quad (5)$$

Nanocavity enhancement of upconverted emission from TTA ($EF_{UCem}$) thus depends on multiple processes, and the relative importance of frequently invoked absorption and emission enhancement mechanisms merits exploration.

Upconverted emission from control samples (silver and cube on quartz, Figure 3g) suggests that nanogap cavity effects are distinct from effects of either the silver mirror or silver nanocubes alone. While these control samples resulted in moderate increases to emission brightness (EF = 6 for silver and EF ≤ 8 for cube on quartz), neither came close to the 35-fold emission enhancement observed for nanogap cavity samples. Metal films have long been used to increase emission brightness by engineering radiative decay rates and directing emission through interactions between oscillating molecular dipoles and metal electrons.[46] In a nanogap cavity, however, the metal film plasmon and the nanocube plasmon hybridize, and the dipole−film interactions are altered.[32] Similarly, emission brightness enhancements in the presence of metal nanoparticles are often attributed to nanoparticle scattering.[42] Due to interactions between the nanoparticle and metal film, however, nanogap cavity-coated surfaces do not scatter light and instead exhibit spectra with intense, narrow absorption bands.[29] Thus, emission enhancement mechanisms present in either the metal film or the silver nanocube alone are superseded by effects of the gap-plasmon mode.

Nanogap cavities aligned with molecular emission transitions, *i.e.* $\lambda_c = \lambda_{em}$, have previously been shown to increase emission brightness by shortening $\tau_{sp}$ and increasing $\Phi_{em}$.[19,20,33] Cavity-coated surfaces resonant with $\lambda_{em}$ used herein, however, produce relatively small upconversion emission brightness enhancement with EF ≈ 15. In cavity-coated surfaces, BPEA $\tau_{sp}$ is only moderately shortened, with $\tau_{sp}^0/\tau_{sp}$ values at most ~7. Further, $\tau_{sp}^0/\tau_{sp}$ is similar for cavity-coated and silver surfaces. This suggests the shortened $\tau_{sp}$ from cavity-coated surfaces might result in part from shortened $\tau_{nr}$ rather than $\tau_r$.[19] Though cavity integration complicates quantification of absorption and thus prevents formal $\Phi_{em}$ measurement within the cavities,[46] finite element simulations of emission from nanogap cavities with $\lambda_c = \lambda_{em}$ provide relevant estimates (see Methods).[19] Here, $\tau_{sp}$ is modeled according to

$$\frac{1}{\tau_{sp}(r)} \propto |\vec{\mathbf{p}}_{BPEA}|^2\rho(r) \quad (6)$$

where $r$ is the position of the dipole, $\vec{\mathbf{p}}_{BPEA}$ is the dipole moment of the BPEA molecule, and $\rho(r)$ is the local density of electromagnetic states which is enhanced by the cavity electric field.[18,41] Assuming BPEA is oriented in the plane of the silver mirror (see Supporting Information (SI)), simulations predict BPEA $\Phi_{em}$ ~ 0.31 in nanogap cavity-coated surfaces (Figure S11, Table S4). Though BPEA solutions display near unity $\Phi_{em}$,[47,48] yields are lessened significantly in thin films.[49] As such, the simulated $\Phi_{em}$ ~ 0.31 represents a small enhancement relative to the $\Phi_{em}^0 = 0.23 \pm 0.02$ measured for BPEA in PMMA thin films on quartz (see Methods). These simulations paired with experimentally observed small $\tau_{sp}^0/\tau_{sp}$ and EF from cavity-coated surfaces resonant with $\lambda_{em}$ suggest that BPEA emission acceleration is not a primary driver of upconversion


https://doi.org/10.1021/acsnano.3c08915
ACS Nano XXXX, XXX, XXX−XXX

emission brightness enhancement. This is consistent with previous reports that decreased $\tau_{sp}$ results in increased emission brightness from some fluorophores through enabling rapid re-excitation.[28] For TTA UC, emissive BPEA is generated through energy transfer and TTA rather than direct excitation, and thus, the influence of shortened $\tau_{sp}$ is limited.

These full-wave simulations of BPEA emission also predict that the collection efficiency $\eta$ should be slightly decreased for cavity-coated surfaces relative to quartz samples for a 0.45 NA objective (Figure S12, Table S4, Methods). Previous reports have shown $\eta/\eta^0$ enhancement to be large for vertically oriented dipole emitters in nanogap cavities (Figure S12),[19] but this effect is significantly lessened for horizontally oriented emitters such as BPEA oriented in the plane of the silver film. In this case simulations suggest both quartz and cavity substrates radiate primarily toward the objective (Figure S12) such that $\eta$ = 0.43 and $\eta^0$ = 0.54 (Table S4). Collection efficiency is not suspected to be significantly improved upon integration of TTA molecules into nanogap cavities, and $\eta$ enhancement is thus not a primary driver of upconversion emission brightness.

Nanogap cavities aligned with molecular absorption transitions, $\lambda_c = \lambda_{abs}$, have previously been shown to increase emission brightness by acting as antennas and increasing the number of excited states formed in a given time ($\kappa_{abs}$) for a given incident light power.[18,33] Herein, upconversion emission brightness is maximized when $\lambda_c = \lambda_{abs}$, which suggests absorption enhancement to be a significant active mechanism. To verify this, $\kappa_{abs}$ is simulated according to

$$\kappa_{abs} \propto |\vec{\mathbf{p}}_{Pt(TPBP)} \cdot \vec{E}|^2 \quad (7)$$

where $\vec{\mathbf{p}}_{Pt(TPBP)}$ is the Pt(TPBP) dipole moment, and $\vec{E}$ is the electric field at the position of the molecule upon 633 nm light excitation.[33,41] In this case, $\kappa_{abs}$ is simulated assuming an isotropic distribution of molecules (see Methods). Though Pt(TPBP) has been observed to self-orient,[50] herein Pt(TPBP) concentrations are low, and absorbance spectra display no broadening indicative of aggregation (Figure 1c).[27] Simulations predict $\kappa_{abs}/\kappa_{abs}^0 \approx 252$, where the majority of excitation enhancement results from Pt(TPBP) molecules aligned vertically between the nanocube and silver mirror (Figure S13). This indicates that absorption enhancement is more than sufficient to account for the experimental EF = 35 for cavity-coated surfaces resonant with $\lambda_{abs}$. Further, simulations predict this absorption enhancement to be a far more significant source of UC emission brightness enhancement than the previously considered effects, consistent with the experimental observation that EF is maximized in cavities resonant with $\lambda_{abs}$.

The strong influence of absorption enhancement is consistent with the broadened PLE observed for nanogap cavities with $\lambda_c$ red-shifted from the Pt(TPBP) absorption peak. These cavities improve the in-coupling of incident light at the cavity resonance to increase the absorption rate for transitions at the very edge of the molecular absorption peak, and the effect is magnified by the low absorption probability of these transitions outside of the cavity. The PLE spectra then becomes a weighted sum of the molecule absorption spectrum and the nanogap cavity spectrum. This enables TTA UC emission to be initiated by wavelengths ≤790 nm, 120 nm redder than the 670 nm cut off observed for quartz controls. The broadened PLE naturally results in excitation wavelength dependent enhancement factors, illustrating how considerations beyond cavity structure influence EF. Though the intensity of the TTA UC emission resulting from >670 nm excitation is small relative to the Pt(TPBP) absorption peak, the broadened PLE expands the portion of the spectrum usable for upconversion applications and increases the achievable apparent anti-Stokes shift.

The assignment of increased absorption as the primary driver of TTA UC emission enhancement is reinforced by the different behaviors observed for Pt(TPBP) phosphorescence as a function of $\lambda_c$. In this case, EF and $\tau_{sp}^0/\tau_{sp}$ are both maximized for cavity-coated surfaces resonant with $\lambda_{phos}$, which suggests that a shortened emission lifetime is the predominant mechanism for phosphorescence enhancement. As opposed to BPEA emission, Pt(TPBP) phosphorescence is slow ($\tau_{sp}^0 \approx 1.16\ \mu s$) and results from direct excitation. As such, emission lifetime alteration is large ($\tau_{sp}^0/\tau_{sp}$ = 207), resulting in bright phosphorescence with EF = 65. It should be noted that the Pt(TPBP) phosphorescence $\tau_{sp}^0$ value observed here is shorter than previous literature reports.[40] This may result from imperfect oxygen exclusion by the protective PVA layer, but it does not affect internal lifetime comparisons.

These mechanistic insights not only suggest increased absorption to be the driving mechanism of TTA UC emission brightness enhancement but also indirectly suggest that nanogap cavities influence the energy transfer steps necessary for TTA UC emission. Experimental results and simulations provide estimates of $EF_{UCem}$, $\eta/\eta^0$, $\kappa_{abs}/\kappa_{abs}^0$, and $\Phi_{em}/\Phi_{em}^0$, which allow eqs 4 and 5 to be solved for an estimated value of $f\Phi_{ISC}\Phi_{EnT}\Phi_{TTA}/f\ {}^0\Phi_{ISC}{}^0\Phi_{EnT}{}^0\Phi_{TTA}{}^0 \approx 0.13$. This is a large decrease in efficiency, though the magnitude of this value relies on multiple simulations, each with associated uncertainty. Generally, these simulations suggest that, though overall TTA UC emission brightness is increased 35-fold, some combination of Pt(TPBP) intersystem crossing, BPEA triplet excited state formation, and triplet−triplet annihilation efficiencies are lessened, potentially significantly, for molecules within nanogap cavity-coated surfaces. The relative alteration of each process is unclear and warrants further exploration, but the large phosphorescence increase observed for the TTA molecular pair on cavity-coated surfaces is consistent with lowered $\Phi_{EnT}$, as more emitting Pt(TPBP) states mean fewer can undergo EnT. This presents clear opportunities for brightened TTA UC emission beyond the 35-fold achieved here—the development of TTA UC emission systems which do not suffer energy transfer efficiency decreases in nanogap cavities while maintaining the same absorption enhancement could conceivably increase EF by nearly an order of magnitude.

Relatedly, nanogap cavity-coated surfaces which exhibit resonance peaks aligned with both $\lambda_{abs}$ and $\lambda_{em}$ result in TTA UC emission which is brighter than any cavity-coated surface with a single $\lambda_c$, with EF = 45. Here, a combination of nanogap cavities produced with two sizes of nanocubes create a dual-resonance surface. Increased enhancement in these surfaces is a somewhat unexpected result as the saturation surface coverage of mixed nanocubes is unchanged from that of single-sized nanocubes, and cavities influencing $\tau_{sp}$ and $\kappa_{abs}$ are generally separated by distances larger than energy transfer lengths. Cooperativity between absorption and emission enhancement is only expected when the two processes are colocalized, as may occur for pairs of cubes which touch. The bright emission observed from these surfaces may reflect improved energy


https://doi.org/10.1021/acsnano.3c08915
ACS Nano XXXX, XXX, XXX−XXX

transfer within these cooperative "hot spots," and points toward a potential for even greater TTA UC emission enhancement in cavities which colocalize $\tau_{sp}$ and $\kappa_{abs}$ influence.

## CONCLUSIONS AND OUTLOOK

Nanogap cavities—silver nanocubes separated from a flat silver mirror by a thin polymer layer—enhance triplet−triplet annihilation upconversion emission from a thin film embedded in the gap. Within the cavities, TTA UC emission brightness is enhanced up to 45-fold and the threshold intensity is decreased nearly an order of magnitude. Further, cavities broaden the spectral range capable of initiating TTA UC emission, increasing the apparent anti-Stokes shift and allowing access to a wider portion of the spectrum. This large TTA UC emission enhancement is achieved through thoughtful cavity design: polymer layers prevent quenching by both the silver mirror and oxygen, minimize mode volumes, and maximize field enhancement; and utilization of multiple nanocube sizes allows simultaneous excitation and emission enhancement. Assembly of these nanogap cavities requires no advanced nanofabrication techniques, and bright emission is observed over large areas, i.e., 210 $\mu$m diameter excitation areas at multiple points on a 20 mm$^2$ surface. Further, enhancement is calculated without scaling factors frequently employed to account for the surface coverage densities of the nanocubes.[20,51] As such, the observed enhancement can likely be directly translated to application and presents an important opportunity to further utilize TTA UC for bioimaging, photocatalysis, and photovoltaics.

In addition, tunability of the nanogap cavity resonance allows selective influence of absorption and emission to probe the efficacy of the overall enhancement mechanism. This experimental cavity tunability paired with finite element simulations shows increased absorption to be the primary mechanism of TTA UC emission enhancement. The ability to distinguish this active mechanism reveals design rules for future TTA UC emission enhancement and illustrates the importance of tailoring the plasmonic nanostructure design to the specific desired process.

The nanogap cavities employed herein, however, are limited to targeting emission and absorption transitions, and simulations suggest that energy transfer steps necessary for TTA UC are hindered in cavity-coated surfaces. Utilization of tethered TTA UC molecular pairs[5] or colocalization of the two cavity resonances, as has been shown to occur for dual mode nanoparticles,[52,53] might decrease this limitation. Further, strong coupling between light-matter states has been shown to enhance energy transfer and nonlinearity in polymer dyes[54−56] and to enhance TTA through modulating the energy of the final singlet state.[23,57] A combined approach utilizing strategies such as these in addition to electronic transition enhancement might allow TTA UC emission to be even brighter than the 45-fold enhancement observed here.

## METHODS

**Sample Fabrication.** Nanocube-coated surfaces were fabricated on a polished prime silicon wafer (⟨1−0−0⟩, 525 $\mu$m thickness, P/B doped). Silver mirrors (80 nm thickness including a 5 nm titanium adhesion layer) with <1 nm RMS roughness were deposited by electron-beam evaporation. Silvered wafers were stored under vacuum until further fabrication steps were taken. Substrates were portioned into ∼1 cm$^2$ pieces and sonicated in IPA for 15 min to remove surface contamination. Quartz slides utilized for control samples were cleaned in the same way.

Triplet−triplet annihilation (TTA) thin films were fabricated from chemicals used as received without further purification. Cleaned silver or quartz substrates were spin coated with ∼6 nm poly(vinyl alcohol) (PVA, Aldrich, MW 89,000−98,000). Polymer film thickness was controlled through the PVA concentration of the spin coated solution. Here, 0.18% aqueous PVA solutions resulted in ∼6 nm films, as measured by imaging ellipsometry (Accurion nanofilm_ep4) when spun at 2600 rpm for 2 min. This layer greatly reduced quenching by the silver surface. Absorbers and emitters known to perform TTA were spin coated onto this PVA layer in a poly(methyl methacrylate) (PMMA, Aldrich, MW ∼ 120,000) matrix. Platinum(II) 5,10,15,20-tetraphenyltetrabenzoporphyrin (Pt(TPBP), BOC Sciences), 9,10-bis(phenylethynyl)anthracene (BPEA, Sigma-Aldrich), and PMMA were dissolved in anisole (Sigma-Aldrich) to concentrations of 0.3 mM, 3 mM, and 3 mg/mL, respectively. Spin coating 750 rpm for 15 s followed by 1500 rpm for 1 min resulted in ∼6 nm films. Samples were dried for 1 h at 80 °C.

Quartz control samples were then finished by spin coating a thick PVA coat (5% aqueous PVA by weight spun at 2000 rpm for 1 min) and stored under a vacuum to exclude oxygen. Nanocube deposition continued by immersing the sample for 2 min in an aqueous solution of 3 mM poly(allylamine hydrochloride) (PAH, Aldrich, MW 17,500) and 1 M sodium chloride (NaCl, Macron), resulting in *in situ* growth of an ∼1 nm cationic PAH polymer layer. Growth was quenched by 1 min of submersion in aqueous 1 M NaCl. Silver nanocubes (45−150 nm) capped with anionic polyvinylpyrrolidone (55 kDa) and stored in ethanol were acquired from nanoComposix, Inc. Nanocubes were resuspended in water and concentrated to 4 mg/mL. For dual-cube samples, equal proportions of 65 and 100 nm cube solutions were combined to yield a final concentration of 2 mg/mL for each size (4 mg/mL total). A 5.0 $\mu$L droplet of the solution was drop-cast onto the sample substrate under a 5 mm diameter round cover glass. The sample was then incubated at 8 °C for 1 h as previously described.[28,29] A randomly oriented layer of silver nanocubes adhered electrostatically to the PAH layer, and excess nanocubes were washed away with water. Nanocubes were imaged by scanning electron microscopy (Apreo S by ThermoFisher Scientific).

**Optical Measurements.** Apart from BPEA $\Phi_{em}$ measurements, all optical measurements were carried out in a reflectance mode at room-temperatures using custom-built microscopes with a 20×, NA = 0.45 objective (∼1.10 mm field-of-view) (Figure S4). Light reached the samples at normal incidence, and reflected light (for both white light reflectance and PL spectrum measurements) was collected through the same objective and measured by using a Horiba iHR550 spectrometer and Horiba Symphony CCD detector. Within the same microscope apparatus, samples were imaged using an Andor Zyla CCD camera. Reflectance spectra were measured using free-space broadband excitation with a tungsten-halogen lamp (ThorLabs). Photoluminescence (PL) spectra were measured using continuous-wave 633 nm He−Ne laser excitation focused to ∼210 $\mu$m diameter at the fwhm. This 210 $\mu$m diameter circle is used to determine the excitation power/area. Alternatively, PLE spectra measured as a function of excitation wavelength were generated using pulsed (∼200 fs, 80 MHz) excitation resulting from second harmonic generation from a tunable OPO pumped with a Ti:sapphire laser (Coherent, Chameleon). Incident power was 200 $\mu$W (580 mW/cm$^2$) unless otherwise noted. PL was collected through the same objective using a 50:50 beam splitter with a coating optimized for 350−1100 nm light. Upconversion emission and phosphorescence were measured independently and isolated by filtering light prior to the spectrometer entrance. The UC emission was isolated with a 633 nm notch filter and a 600 nm short pass filter. Phosphorescence was isolated using a 633 nm notch filter and a 715 nm long pass filter. Photoluminescence areas were integrated to determine enhancement factors, intensity thresholds, and PL magnitudes for PLE spectra over set spectral ranges: 500−580 nm for BPEA emission and 725−825 for Pt(TPBP) phosphorescence.


https://doi.org/10.1021/acsnano.3c08915
ACS Nano XXXX, XXX, XXX−XXX

Kinetic measurements were carried out in a similar microscope apparatus using femtosecond pulsed laser excitation (Coherent Monaco) (Figure S8). The laser was filtered prior to the sample to ensure a monochromatic excitation. Concomitant reflectance and PL spectra were measured by using an Andor spectrograph fitted with an iDus CCD. BPEA decay lifetimes in Figure 3e were measured using 440 nm pulsed excitation, 50 kHz repetition rate, and 4 $\mu$W power. Excitation with 440 nm light directly excites BPEA, which removes the kinetic complication of the prerequisite energy transfer. Equivalent results were acquired for active layers of BPEA alone and those of BPEA and Pt(TPBP) together. Pt(TPBP) phosphorescence decay lifetimes in Figure 6b were measured using 633 nm pulsed excitation, 10 kHz repetition rate, and 10 $\mu$W power. BPEA emission and Pt(TPBP) phosphorescence were captured through the microscope objective using appropriate dichroic mirrors (505 and 650 nm long pass, respectively). Prior to photon detection, BPEA emission was isolated with a 500 nm long pass filter and 600 nm short pass filter. Pt(PTBP) phosphorescence was isolated with a 633 nm notch filter and a 715 nm long pass filter. Lifetimes were measured using a free-space Avalanche Photodiode (Micro Photon Devices, PDM Series) coupled to a Time-Correlated Single Photon Counting module (PicoQuant Multiharp) that recorded the photon arrival time relative to a trigger by the laser pulse. Kinetic data were well-modeled by a Kohlrausch–Williams–Watts function (eq 8), where $I$ is the emission intensity, $\tau$ is the emission lifetime, and $\beta$ is a stretching parameter between 0 and 1.[37,38]

$$I(t) = I_0 e^{-\left(\frac{t}{\tau}\right)^{\beta}} \tag{8}$$

Average lifetimes, which were taken as approximations of the spontaneous emission lifetime, $\tau_{sp}$, were extracted as the first moment of a Lévy distribution (eq 9), where $\Gamma$ is the gamma function.

$$\tau_{sp} = \frac{1}{\tau}\frac{\beta}{\Gamma\left(\frac{1}{\beta}\right)} \tag{9}$$

So that $\tau_{sp}$ values could be compared between experiments, data for BPEA emission and Pt(TPBP) phosphorescence were first fit to find the best $\beta$ for each individual experiment. These values of $\beta$ were then averaged for each process ($\beta$ = 0.42 for BPEA emission, and $\beta$ = 0.39 for Pt(TPBP) phosphorescence). Data were fit again with this average value, and these $\tau_{sp}$ values were reported.

The emission quantum yield for BPEA on quartz was measured using a procedure modified from previous literature.[58,59] Briefly, 3 mM BPEA was dissolved in a 75 mg/mL PMMA anisole solution and spin coated onto a quartz substrate to produce an ~120 nm thin film. These films were created to be thicker than the PMMA layers used in nanogap cavities so that absorbance could be reliably quantified. PMMA films were coated in ~500 nm PVA spin coated from a 5 wt % aqueous PVA solution and dried in vacuum overnight. Samples were mounted at the input port of an integrating sphere, which was fiber-coupled to a Horiba iHR550 spectrometer and Horiba Symphony CCD detector calibrated with a tungsten-halogen lamp. Transmittance of a 440 nm CW laser and emission were quantified for PMMA films on quartz with and without BPEA. Quantum yield was then calculated according to

$$\Phi_{em} = \frac{\int (CPS_{em}^{BPEA}(\lambda) - CPS_{em}^{ref}(\lambda))\, d\lambda}{\int (CPS_{ex}^{ref}(\lambda) - CPS_{ex}^{BPEA}(\lambda))\, d\lambda} \tag{10}$$

where $CPS$ is counts per second measured by the spectrometer, superscripts $BPEA$ and $ref$ refer to BPEA on quartz samples and PMMA with no BPEA on quartz reference samples, and the subscripts $em$ and $ex$ indicate measurement of emitted light or transmitted excitation light.

**Finite Element Simulations.** Finite-element simulations were conducted to simulate the electric field distribution upon light excitation within the plasmonic nanogap cavities as described previously.[60] Simulations were conducted in COMSOL Multiphysics using the Wave Optics module in the frequency domain. Geometric conditions equivalent to experimental samples for nanogap cavities resonant with $\lambda_{abs}$ were employed (100 nm side length), and nanocubes were rounded with a radius of 10% of the side length. Periodic boundary conditions in the $x$–$y$ plane and perfectly matched layers along the $z$ axis simulated an infinite array of individual nanogap cavities, which approximated a conformally covered surface. Absorption enhancement was calculated according to eq 7 where assumption of an isotropic Pt(TPBP) distribution allows $\vec{p}_{Pt(TPBP)}$ to be treated as an unit vector integrated over a sphere.

Additional finite element simulations (COMSOL) were performed to simulate BPEA emission as described previously.[18,41,61] A single nanogap cavity with geometric conditions equivalent to experimental samples resonant with $\lambda_{em}$ (60 nm side length) with rounded corners was modeled in a spherical domain with scattering boundary conditions. All materials were modeled according to known permittivity values.[62] The BPEA molecule was modeled as a 530 nm emitting point dipole placed on a 13 × 13 grid in a plane 6 nm below the nanocube, and 4-fold symmetry was assumed to reduce computational demands. Average values presented in the text were generated by averaging across the grid, encompassing both nanocube-coupled and uncoupled areas to approximate a surface with ~20% nanocube surface coverage. The Green's function of the system was used to numerically simulate radiative and nonradiative decay rates as described in ref 61, which were used to calculate $\Phi_{em}$ according to eq 3. Collection efficiencies were calculated within these simulations as the ratio of power radiated at the scattering boundary for a portion of the hemisphere corresponding to a 0.45 NA objective to the total radiated power,[18] and radiation patterns were visualized using the open-source near-to-far-field transformation package RETOP.[63] Separate simulations were performed for dipoles oriented on the three Cartesian coordinates and at 45° between the three axes. Because simulated emission parameters matched much more closely to experimental $\tau_{sp}^0/\tau_{sp}$ values for dipoles oriented along $x$ and $y$ and in the $xy$ plane (see SI, Table S4), these simulations were averaged to generate the reported values, while dipoles oriented in $z$ were excluded.

## ASSOCIATED CONTENT

### Supporting Information

The Supporting Information is available free of charge at https://pubs.acs.org/doi/10.1021/acsnano.3c08915.

Experimental setup schemes, additional PL and reflectance spectra, nanocube on quartz reflectance spectra, EF as a function of excitation wavelength, long time scale phosphorescence kinetics, finite element simulations. (PDF)

## AUTHOR INFORMATION


### Corresponding Author

**Maiken H. Mikkelsen** − *Department of Electrical and Computer Engineering, Duke University, Durham, North Carolina 27708, United States;* orcid.org/0000-0002-0487-7585; Email: m.mikkelsen@duke.edu

### Authors

**Rachel E. Bangle** − *Department of Electrical and Computer Engineering, Duke University, Durham, North Carolina 27708, United States*

**Hengming Li** − *Department of Electrical and Computer Engineering, Duke University, Durham, North Carolina 27708, United States*

Complete contact information is available at: https://pubs.acs.org/doi/10.1021/acsnano.3c08915




https://doi.org/10.1021/acsnano.3c08915
ACS Nano XXXX, XXX, XXX−XXX

### Funding

Funding by the Air Force Office of Scientific Research, the Arnold and Mabel Beckman Foundation, and the National Science Foundation Graduate Research Fellowship Program is acknowledged.

### Notes

The authors declare no competing financial interest.

## ACKNOWLEDGMENTS

This work was supported by the Air Force Office of Scientific Research (AFOSR), grant # FA9550-21-1-0312. Additionally, R.E.B. acknowledges support from the Arnold O. Beckman Postdoctoral Fellowship and H.L. acknowledges support from the National Science Foundation Graduate Research Fellowship. This work was performed in part using instrumentation at the Duke University Shared Materials Instrumentation Facility (SMIF). This work was also performed in part using instrumentation at the Chapel Hill Analytical and Nanofabrication Laboratory, CHANL. Both SMIF and CHANL are members of the North Carolina Research Triangle Nanotechnology Network (RTNN), which is supported by the National Science Foundation (Grant ECCS-1542015), as part of the National Nanotechnology Coordinated Infrastructure (NNCI).

## ABBREVIATIONS

BPEA, bis(phenylethynyl)anthracene; EF, enhancement factor; PAH, poly(allylamine hydrochloride); PL, photoluminescence; PLE, photoluminescence excitation; PMMA, poly(methyl methacrylate); Pt(TPBP), 5,10,15,20-(tetraphenyl)-tetrabenzoporphyin; PVA, poly(vinyl alcohol); PVP, polyvinylpyrrolidone; $S_1$, singlet state; SEM, scanning electron microscopy; $T_1$, triplet state; TTA, triplet−triplet annihilation; UC, upconversion

## REFERENCES

(1) Singh-Rachford, T. N.; Castellano, F. N. Photon Upconversion Based on Sensitized Triplet-Triplet Annihilation. *Coord. Chem. Rev.* **2010**, *254* (21−22), 2560−2573.

(2) Zhao, J.; Ji, S.; Guo, H. Triplet-Triplet Annihilation Based Upconversion: From Triplet Sensitizers and Triplet Acceptors to Upconversion Quantum Yields. *RSC Adv.* **2011**, *1* (6), 937−950.

(3) Zhou, J.; Liu, Q.; Feng, W.; Sun, Y.; Li, F. Upconversion Luminescent Materials: Advances and Applications. *Chem. Rev.* **2015**, *115* (1), 395−465.

(4) Wu, D. M.; García-Etxarri, A.; Salleo, A.; Dionne, J. A. Plasmon-Enhanced Upconversion. *J. Phys. Chem. Lett.* **2014**, *5* (22), 4020−4031.

(5) Zeng, L.; Huang, L.; Han, J.; Han, G. Enhancing Triplet-Triplet Annihilation Upconversion: From Molecular Design to Present Applications. *Acc. Chem. Res.* **2022**, *55* (18), 2604−2615.

(6) Carrod, A. J.; Gray, V.; Börjesson, K. Recent Advances in Triplet-Triplet Annihilation Upconversion and Singlet Fission, towards Solar Energy Applications. *Energy Environ. Sci.* **2022**, *15* (12), 4982−5016.

(7) Gao, C.; Wong, W. W. H.; Qin, Z.; Lo, S.; Namdas, E. B.; Dong, H.; Hu, W. Application of Triplet-Triplet Annihilation Upconversion in Organic Optoelectronic Devices: Advances and Perspectives. *Adv. Mater.* **2021**, *33* (45), 2100704.

(8) Huang, L.; Wu, W.; Li, Y.; Huang, K.; Zeng, L.; Lin, W.; Han, G. Highly Effective Near-Infrared Activating Triplet-Triplet Annihilation Upconversion for Photoredox Catalysis. *J. Am. Chem. Soc.* **2020**, *142* (43), 18460−18470.

(9) Huang, L.; Le, T.; Huang, K.; Han, G. Enzymatic Enhancing of Triplet-Triplet Annihilation Upconversion by Breaking Oxygen Quenching for Background-Free Biological Sensing. *Nat. Commun.* **2021**, *12* (1), 1−9.

(10) Yang, D.; Ma, P.; Hou, Z.; Cheng, Z.; Li, C.; Lin, J. Current Advances in Lanthanide Ion ($Ln^{3+}$)-Based Upconversion Nanomaterials for Drug Delivery. *Chem. Soc. Rev.* **2015**, *44* (6), 1416−1448.

(11) Sanders, S. N.; Schloemer, T. H.; Gangishetty, M. K.; Anderson, D.; Seitz, M.; Gallegos, A. O.; Stokes, R. C.; Congreve, D. N. Triplet Fusion Upconversion Nanocapsules for Volumetric 3D Printing. *Nature.* **2022**, *604* (7906), 474−478.

(12) Schmidt, T. W.; Castellano, F. N. Photochemical Upconversion: The Primacy of Kinetics. *J. Phys. Chem. Lett.* **2014**, *5* (22), 4062−4072.

(13) Bharmoria, P.; Bildirir, H.; Moth-Poulsen, K. Triplet-Triplet Annihilation Based near Infrared to Visible Molecular Photon Upconversion. *Chem. Soc. Rev.* **2020**, *49* (18), 6529−6554.

(14) Islangulov, R. R.; Lott, J.; Weder, C.; Castellano, F. N. Noncoherent Low-Power Upconversion in Solid Polymer Films. *J. Am. Chem. Soc.* **2007**, *129* (42), 12652−12653.

(15) Jiang, X.; Guo, X.; Peng, J.; Zhao, D.; Ma, Y. Triplet-Triplet Annihilation Photon Upconversion in Polymer Thin Film: Sensitizer Design. *ACS Appl. Mater. Interfaces* **2016**, *8* (18), 11441−11449.

(16) Gray, V.; Moth-Poulsen, K.; Albinsson, B.; Abrahamsson, M. Towards Efficient Solid-State Triplet-Triplet Annihilation Based Photon Upconversion: Supramolecular, Macromolecular and Self-Assembly Systems. *Coord. Chem. Rev.* **2018**, *362*, 54−71.

(17) Beery, D.; Schmidt, T. W.; Hanson, K. Harnessing Sunlight via Molecular Photon Upconversion. *ACS Appl. Mater. Interfaces* **2021**, *13* (28), 32601−32605.

(18) Rose, A.; Hoang, T. B.; Mcguire, F.; Mock, J. J.; Ciracì, C.; Smith, D. R.; Mikkelsen, M. H. Control of Radiative Processes Using Tunable Plasmonic Nanopatch Antennas. *Nano Lett.* **2014**, *14*, 4797−4802.

(19) Akselrod, G. M.; Argyropoulos, C.; Hoang, T. B.; Ciracì, C.; Fang, C.; Huang, J.; Smith, D. R.; Mikkelsen, M. H. Probing the Mechanisms of Large Purcell Enhancement in Plasmonic Nanoantennas. *Nat. Photonics* **2014**, *8* (11), 835−840.

(20) Wu, Y.; Xu, J.; Poh, E. T.; Liang, L.; Liu, H.; Yang, J. K. W.; Qiu, C. W.; Vallée, R. A. L.; Liu, X. Upconversion Superburst with Sub-2 μs Lifetime. *Nat. Nanotechnol.* **2019**, *14* (12), 1110−1115.

(21) Jin, S.; Sugawa, K.; Takeshima, N.; Tahara, H.; Igari, S.; Yoshinari, S.; Kurihara, Y.; Watanabe, S.; Enoki, M.; Sato, K.; Inoue, W.; Tokuda, K.; Akiyama, T.; Katoh, R.; Takase, K.; Ozawa, H.; Okazaki, T.; Watanabe, T.; Otsuki, J. Precise Control of Localized Surface Plasmon Wavelengths Is Needed for Effective Enhancement of Triplet-Triplet Annihilation-Based Upconversion Emission. *ACS Photonics* **2018**, *5* (12), 5025−5037.

(22) Poorkazem, K.; Hesketh, A. V.; Kelly, T. L. Plasmon-Enhanced Triplet-Triplet Annihilation Using Silver Nanoplates. *J. Phys. Chem. C* **2014**, *118* (12), 6398−6404.

(23) Ye, C.; Mallick, S.; Hertzog, M.; Kowalewski, M.; Börjesson, K. Direct Transition from Triplet Excitons to Hybrid Light-Matter States via Triplet-Triplet Annihilation. *J. Am. Chem. Soc.* **2021**, *143* (19), 7501−7508.

(24) Wu, M.; Lin, T. A.; Tiepelt, J. O.; Bulović, V.; Baldo, M. A. Nanocrystal-Sensitized Infrared-to-Visible Upconversion in a Microcavity under Subsolar Flux. *Nano Lett.* **2021**, *21* (2), 1011−1016.

(25) Zhou, H.; Lin, J.; Wan, S.; Lu, W. Photochemically Deoxygenating Gels for Triplet-Triplet Annihilation Photon-Upconversion Performed under Air. *Phys. Chem. Chem. Phys.* **2022**, *24* (47), 29151−29158.

(26) Roberts, S. T.; Schlenker, C. W.; Barlier, V.; McAnally, R. E.; Zhang, Y.; Mastron, J. N.; Thompson, M. E.; Bradforth, S. E. Observation of Triplet Exciton Formation in a Platinum-Sensitized Organic Photovoltaic Device. *J. Phys. Chem. Lett.* **2011**, *2* (2), 48−54.

(27) Mongin, C.; Golden, J. H.; Castellano, F. N. Liquid PEG Polymers Containing Antioxidants: A Versatile Platform for Studying Oxygen-Sensitive Photochemical Processes. *ACS Appl. Mater. Interfaces* **2016**, *8* (36), 24038−24048.



https://doi.org/10.1021/acsnano.3c08915
*ACS Nano* XXXX, XXX, XXX−XXX

(28) Hoang, T. B.; Huang, J.; Mikkelsen, M. H. Colloidal Synthesis of Nanopatch Antennas for Applications in Plasmonics and Nanophotonics. *J. Vis. Exp.* **2016**, *2016* (111), 53876.
(29) Akselrod, G. M.; Huang, J.; Hoang, T. B.; Bowen, P. T.; Su, L.; Smith, D. R.; Mikkelsen, M. H. Large-Area Metasurface Perfect Absorbers from Visible to Near-Infrared. *Adv. Mater.* **2015**, *27* (48), 8028−8034.
(30) Moreau, A.; Ciracì, C. C.; Mock, J. J.; Hill, R. T.; Wang, Q.; Wiley, B. J.; Chilkoti, A.; Smith, D. R. Controlled-Reflectance Surfaces with Film-Coupled Colloidal Nanoantennas. *Nature* **2012**, *492* (7427), 86−89.
(31) Bowen, P. T.; Baron, A.; Smith, D. R. Theory of Patch-Antenna Metamaterial Perfect Absorbers. *Phys. Rev. A* **2016**, *93* (6), 063849.
(32) Bowen, P. T.; Smith, D. R. Coupled-Mode Theory for Film-Coupled Plasmonic Nanocubes. *Phys. Rev. B* **2014**, *90* (19), 195402.
(33) Baumberg, J. J.; Aizpurua, J.; Mikkelsen, M. H.; Smith, D. R. Extreme Nanophotonics from Ultrathin Metallic Gaps. *Nat. Mater.* **2019**, *18* (7), 668−678.
(34) Wiley, B.; Sun, Y.; Xia, Y. Synthesis of Silver Nanostructures with Controlled Shapes and Properties. *Acc. Chem. Res.* **2007**, *40* (10), 1067−1076.
(35) Sun, Y.; Xia, Y. Shape-Controlled Synthesis of Gold and Silver Nanoparticles. *Science.* **2002**, *298* (5601), 2176−2179.
(36) Abulikemu, A.; Sakagami, Y.; Heck, C.; Kamada, K.; Sotome, H.; Miyasaka, H.; Kuzuhara, D.; Yamada, H. Solid-State, Near-Infrared to Visible Photon Upconversion via Triplet-Triplet Annihilation of a Binary System Fabricated by Solution Casting. *ACS Appl. Mater. Interfaces* **2019**, *11* (23), 20812−20819.
(37) Williams, G.; Watts, D. C. Non-Symmetrical Dielectric Relaxation Behaviour Arising from a Simple Empirical Decay Function. *Trans. Faraday Soc.* **1970**, *66* (1), 80−85.
(38) Berberan-Santos, M. N.; Bodunov, E. N.; Valeur, B. Mathematical Functions for the Analysis of Luminescence Decays with Underlying Distributions 1. Kohlrausch Decay Function (Stretched Exponential). *Chem. Phys.* **2005**, *315* (1−2), 171−182.
(39) Kinkhabwala, A.; Yu, Z.; Fan, S.; Avlasevich, Y.; Müllen, K.; Moerner, W. E. Large Single-Molecule Fluorescence Enhancements Produced by a Bowtie Nanoantenna. *Nat. Photonics* **2009**, *3* (11), 654−657.
(40) Russell, K. J.; Liu, T.-L.; Cui, S.; Hu, E. L. Large Spontaneous Emission Enhancement in Plasmonic Nanocavities. *Nat. Photonics.* **2012**, *6* (7), 459−462.
(41) Anger, P.; Bharadwaj, P.; Novotny, L. Enhancement and Quenching of Single-Molecule Fluorescence. *Phys. Rev. Lett.* **2006**, *96*, 113002.
(42) Li, K.; Hogan, N. J.; Kale, M. J.; Halas, N. J.; Nordlander, P.; Christopher, P. Balancing Near-Field Enhancement, Absorption, and Scattering for Effective Antenna-Reactor Plasmonic Photocatalysis. *Nano Lett.* **2017**, *17* (6), 3710−3717.
(43) Jauffred, L.; Samadi, A.; Bendix, P. M.; Oddershede, L. B. Plasmonic Heating of Nanostructures. *Chem. Rev.* **2019**, *119* (13), 8087−8130.
(44) Gray, V.; Dzebo, D.; Abrahamsson, M.; Albinsson, B.; Moth-Poulsen, K. Triplet-Triplet Annihilation Photon-Upconversion: Towards Solar Energy Applications. *Phys. Chem. Chem. Phys.* **2014**, *16* (22), 10345−10352.
(45) Zhou, Y.; Castellano, F. N.; Schmidt, T. W.; Hanson, K. On the Quantum Yield of Photon Upconversion via Triplet-Triplet Annihilation. *ACS Energy Lett.* **2020**, *5* (7), 2322−2326.
(46) Lakowicz, J. R. Radiative Decay Engineering: Biophysical and Biomedical Applications. *Anal. Biochem.* **2001**, *298* (1), 1−24.
(47) Heller, C. A.; Henry, R. A.; McLaughlin, B. A.; Bliss, D. E. Fluorescence Spectra and Quantum Yields: Quinine, Uranine, 9,10-Diphenylanthracene, and 9,10-Bis(Phenylethynyl)Anthracenes. *J. Chem. Eng. Data* **1974**, *19* (3), 214−219.
(48) Demeter, A. First Steps in Photophysics. I. Fluorescence Yield and Radiative Rate Coefficient of 9,10-Bis(Phenylethynyl)Anthracene in Paraffins. *J. Phys. Chem. A* **2014**, *118* (43), 9985−9993.
(49) Manna, B.; Nandi, A.; Ghosh, R. Ultrafast Singlet Exciton Fission Dynamics in 9,10-Bis(Phenylethynyl)Anthracene Nanoaggregates and Thin Films. *J. Phys. Chem. C* **2018**, *122* (36), 21047−21055.
(50) Medforth, C. J.; Wang, Z.; Martin, K. E.; Song, Y.; Jacobsen, J. L.; Shelnutt, J. A. Self-Assembled Porphyrin Nanostructures. *Chem. Commun.* **2009**, *47*, 7261.
(51) Hoang, T. B.; Akselrod, G. M.; Argyropoulos, C.; Huang, J.; Smith, D. R.; Mikkelsen, M. H. Ultrafast Spontaneous Emission Source Using Plasmonic Nanoantennas. *Nat. Commun.* **2015**, *6* (1), 1−7.
(52) Shen, Q.; Boyce, A. M.; Yang, G.; Mikkelsen, M. H. Polarization-Controlled Nanogap Cavity with Dual-Band and Spatially Overlapped Resonances. *ACS Photonics* **2019**, *6* (8), 1916−1921.
(53) Xomalis, A.; Zheng, X.; Chikkaraddy, R.; Koczor-Benda, Z.; Miele, E.; Rosta, E.; Vandenbosch, G. A. E.; Martínez, A.; Baumberg, J. J. Detecting Mid-Infrared Light by Molecular Frequency Upconversion in Dual-Wavelength Nanoantennas. *Science.* **2021**, *374* (6572), 1268−1271.
(54) Coles, D. M.; Somaschi, N.; Michetti, P.; Clark, C.; Lagoudakis, P. G.; Savvidis, P. G.; Lidzey, D. G. Polariton-Mediated Energy Transfer between Organic Dyes in a Strongly Coupled Optical Microcavity. *Nat. Mater.* **2014**, *13* (7), 712−719.
(55) Zhong, X.; Chervy, T.; Wang, S.; George, J.; Thomas, A.; Hutchison, J. A.; Devaux, E.; Genet, C.; Ebbesen, T. W. Non-Radiative Energy Transfer Mediated by Hybrid Light-Matter States. *Angew. Chem.* **2016**, *128* (21), 6310−6314.
(56) Fofang, N. T.; Grady, N. K.; Fan, Z.; Govorov, A. O.; Halas, N. J. Plexciton Dynamics: Exciton-Plasmon Coupling in a J-Aggregate-Au Nanoshell Complex Provides a Mechanism for Nonlinearity. *Nano Lett.* **2011**, *11* (4), 1556−1560.
(57) Polak, D.; Jayaprakash, R.; Lyons, T. P.; Martínez-Martínez, L.; Leventis, A.; Fallon, K. J.; Coulthard, H.; Bossanyi, D. G.; Georgiou, K.; Petty, A. J.; Anthony, J.; Bronstein, H.; Yuen-Zhou, J.; Tartakovskii, A. I.; Clark, J.; Musser, A. J. Manipulating Molecules with Strong Coupling: Harvesting Triplet Excitons in Organic Exciton Microcavities. *Chem. Sci.* **2020**, *11* (2), 343−354.
(58) Johnson, A. R.; Lee, S.-J.; Klein, J.; Kanicki, J. Absolute Photoluminescence Quantum Efficiency Measurement of Light-Emitting Thin Films. *Rev. Sci. Instrum.* **2007**, *78*, 096101.
(59) Suzuki, K.; Kobayashi, A.; Kaneko, S.; Takehira, K.; Yoshihara, T.; Ishida, H.; Shiina, Y.; Oishi, S.; Tobita, S. Reevaluation of Absolute Luminescence Quantum Yields of Standard Solutions Using a Spectrometer with an Integrating Sphere and a Back-Thinned CCD Detector. *Phys. Chem. Chem. Phys.* **2009**, *11* (42), 9850.
(60) Stewart, J. W.; Vella, J. H.; Li, W.; Fan, S.; Mikkelsen, M. H. Ultrafast Pyroelectric Photodetection with On-Chip Spectral Filters. *Nat. Mater.* **2020**, *19* (2), 158−162.
(61) Ciracì, C.; Rose, A.; Argyropoulos, C.; Smith, D. R. Numerical Studies of the Modification of Photodynamic Processes by Film-Coupled Plasmonic Nanoparticles. *J. Opt. Soc. Am. B* **2014**, *31* (11), 2601.
(62) Palik, E. D. *Handbook of Optical Constants of Solids*; Academic Press: 1985.
(63) Yang, J.; Hugonin, J.-P.; Lalanne, P. Near-to-Far Field Transformations for Radiative and Guided Waves. *ACS Photonics* **2016**, *3* (3), 395−402.


https://doi.org/10.1021/acsnano.3c08915
*ACS Nano* XXXX, XXX, XXX−XXX